Journal of Civil Engineering
The Institution of Engineers, Bangladesh
Vol. CE 31, No. 2, 2003

DILATANCY CHARACTERISTICS OF A SAND AT CONSTANT STRESS-STATES IN TRIAXIAL COMPRESSION

Eqramul Hoque[1]

ABSTRACT: Deformation characteristics of Hostun sand, French sand, at constant stress-states (often termed as creep) was experimentally investigated using solid cylindrical triaxial specimens equipped with high resolution transducers to measure axial load, axial and radial strains locally. Each specimen, isotropically consolidated by partial vacuum at 78.4 kPa, was subjected to monotonic axial compression segmentally by using an automated load-control system. Each axial stress segment generally consisted of shearing up to the next predetermined axial stress σ_a level, allowing sufficient time to reduce the creep deformation rate to a negligible value while maintaining the current stress state, subsequently loading to the next predetermined σ_a, and so on. It was observed that creep deformation increased with the increase in shear stress level during monotonic loading and the rate was larger in the major principal stress direction compared to other principal stress directions. Creep strain followed Rowe's stress-dilatancy relationship.

KEYWORDS: Triaxial, local-strains, segmental-shear, creep, delayed-rebound, dilatancy

INTRODUCTION

Characterizing creep deformation of soils is important for proper modeling. The creep (or secondary compression in case of clay) deformation results from readjustment of particle contacts at essentially constant effective stresses. Any geotechnical design calculation requires a conscious or unconscious choice of a model of soil behavior. Settlement calculations typically assume that the soil is linear and elastic, and bearing capacity calculations typically assume that the soil is elastic and perfectly plastic. However, these basic models do not get very far; geotechnical constructions under working loads will certainly have proceeded well beyond a linear elastic range and yet are unlikely to have attained conditions of perfect plasticity. In reality, soil is an elasto viscoplastic material and the framework for such models was set up by Perzyna (1963) and Olszak and Perzyna (1966). In this model, the term creep is usually used to describe deformations continuing with time at constant effective stresses. If a soil shows creep deformations, then such creep deformations are occurring all the time, even though they can only be observed when the stresses are held constant. In tests performed at different rates, at any particular stress state different amounts of creep deformation will have

[1] Department of Civil Engineering, BUET, Dhaka-1000, Bangladesh

developed because of the different times that have elapsed, and different stress-strain relationships are observed (Wood, 1990). If the rate of loading is changed in the middle of a test, then it is typically found (e.g., Richardson and Whitman, 1963) that the state of the soil quickly jumps to the stress-strain curve appropriate to the new rate, i.e., the stress-strain curve that would have been followed if it were loaded from the beginning at the new rate. Described herein are creep deformation characteristics of Hostun sand (French sand) that were measured on small solid cylindrical specimens under triaxial stress conditions. Some of these results have been reported in Hoque and Tatsuoka (2003).

THE TRIAXIAL APPARATUS

The experimental works were carried out in an advanced triaxial apparatus (Fig. 1). Unlike conventional triaxial system, it can accommodate high resolution transducers to measure strains less than 10^{-5} with having good long-term stability even when submerged and in which, the deformation characteristics from very small strain to the large strain can be evaluated from multi-stage tests on single specimen (Tatsuoka et al., 1997). The deviator load was measured by a sensitive load cell placed inside the triaxial cell. Local axial strains free from bedding errors were measured by a pair of Local Deformation Transducers LDTs (Goto et al. 1991) hinged vertically on diametrically opposite sides of a specimen surface and local radial strains were measured by using three pairs of gap sensors (GSs) at three levels along the height of the specimen. Besides, a gap sensor (GS) was used to measure the displacement of loading cap (i.e., conventional axial strain measurement) of triaxial apparatus. The pressure was applied inside the voids of soil particles by partial vacuum and the deviator load was applied by air pressure through a two-chambered Bellofram cylinder. An anisotropic compression stress-state (i.e., axial stress σ_a > radial stress σ_r) was achieved by controlling confining pressure and both static and dynamic components of pressure in the Bellofram cylinder.

TEST PROCEDURE

Tests were performed on small cylindrical specimens (7.5 cm diameter and 15 cm high) of Hostun sand. Physical properties of the sand are: D_{10}= 0.17 mm, D_{50}= 0.31 mm, U_c= 1.94, G_s= 2.65, e_{max}= 0.95 and e_{min}= 0.55. Each specimen was reconstituted by raining air-dried sand particles through air into a split mold. Regular ends (i.e., non-lubricated ends using porous stones) were used at both ends of a specimen. A partial vacuum of 10 kPa was applied first to a specimen, which was completely enclosed within a rubber membrane before the mold was dissembled. A free-standing specimen was then consolidated isotropically to a confining pressure σ_c = 78.4 kPa at which the specimen dimensions were measured before any instrumentation.

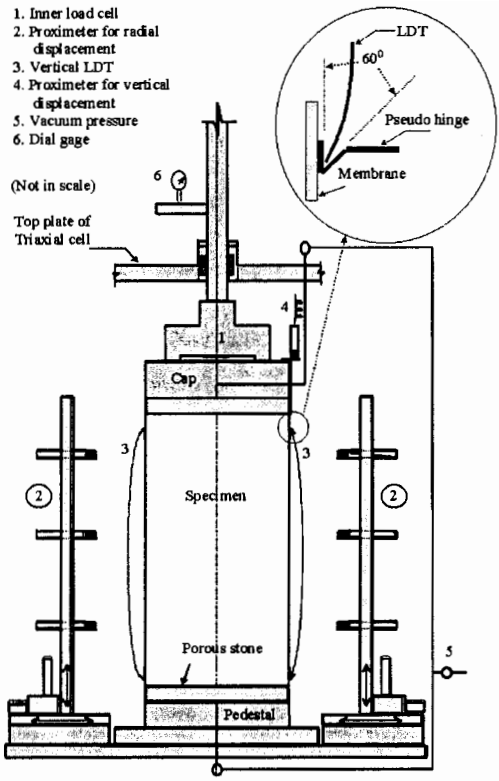

Fig. 1. The triaxial testing system

Tests were conducted on three specimens: HOSTN2 (initial void ratio, e_0= 0.70), HOSTN4 (e_0= 0.88) and HOS12 (e_0= 0.72). The relationships between axial stress (σ_a), axial strain (ε_a) and radial strain (ε_r) obtained by performing multi-stage segmental shear tests in TC on HOS12 are shown, respectively, in Figs. 2a and b. The encircled numbers (e.g., 0, 1, etc.) shown in the figures indicate the stress states at which the specimens were allowed to undergo creep at constant stress state (i.e., creep test), while the number '0' indicating the initial stress point. Each axial stress segment (e.g., segment from 0 to 1 or simply 0-1 in Fig. 2a) generally consisted of the following steps sequentially: (a) shearing up to the next predetermined σ_a level; (b) conducting creep test at the current stress-state; (c) application of very small-amplitude axial cyclic load (CYL) to evaluate small strain stiffness; (d) loading to the next predetermined σ_a, and so on. Besides, a few sub-steps were included in some cases in between steps (c) and (d) aforesaid, namely: (i) unloading to a stress-state in compression

zone (e.g., the segment 2-3 of Fig. 2a); (ii) performing creep test (i.e., delayed rebound) at the over-consolidated stress-state, (iii) reloading to a σ_a value, slightly lower than the previously experienced maximum σ_a, and (iv) the application of very small-amplitude unload-reload cycles at various stress states during reloading. The latter stress-states were shown by using asteric (*) symbol in Fig. 2a and were grouped together by symbols 'A', 'B' and 'C' according to the 'unloading event'.

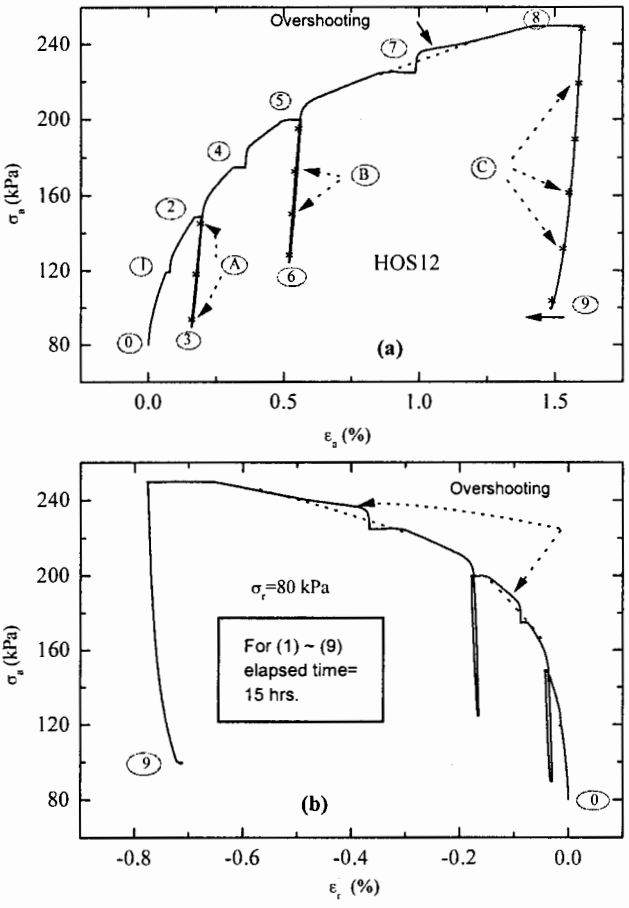

Fig. 2. (a) $\sigma_a \sim \varepsilon_a$, and (b) $\sigma_a \sim \varepsilon_r$ relations in TC on HOS12

In segmental shear, deviator load was applied at a constant rate of axial stress equal to 12.25 kPa/min by increasing the axial stress in very small steps, while in creep test a constant stress-state was

maintained within an accuracy of ±0.25 kPa. All the tests were performed at σ_r = 80 kPa. The maximum stress level during segmental shear was kept well below the failure-state. Table 1 lists test specimens with some results. The entities E_1, m and σ_0 are elastic parameters that are referred later. In Table 1 and following figures (if not otherwise specified), stresses and stiffness are normalized by dividing it with the atmospheric pressure p_a= 98 kPa.

Table 1. List of the specimens and some results (P_a= 98 kPa)

Specimen	e_0	E_1 / p_a	m	ν_0
HOSTN2	0.70	1920	0.47	0.17
HOSTN4	0.88	1890	0.47	0.23
HOS12	0.72	1800	0.48	0.14

RESULTS AND DISCUSSIONS

Axial strains σ_a measured by LDTs on specimen HOS12 are shown in Fig. 2a. The strains measured by GS, generally affected by bedding error and system compliance (Tatsuoka et al., 1997), are available in Hoque (1996). The radial strains σ_r measured by GSs at three levels of a specimen (Fig. 1), on averaging, are shown in Fig. 2b. It can be observed that time-dependent deformation (i.e., creep) occurred at a constant virgin stress state along loading (i.e., $\Delta\sigma_a$ >0) stress path. It also occurred at a constant stress-state in an unloading stress path, which was called 'delayed rebound' because it was the recovery of strain after the recent unloading. The sand appeared to exhibit elastic behaviour at the reloading stress-state of virgin segmental shear after creep deformation reduced to a negligible value; the deformation at the reloading point (e.g., stress-state '1' of segmental shear along 1-2 in Fig. 3a) appeared to be similar to that occurred at the initial part of the 0-1 segment (Fig. 2a). Over-shooting in the stress-strain relationships during a segmental shear was observed in some instances after creep (e.g., 5-7 and 7-8 stress segments, Figs. 2a and b). Here, over-shooting means a stiffer response compared to the response that would occur during monotonic loading at the same stress-state in otherwise similar conditions (i.e., without allowing creep to occur). The behaviour was not, however, observed at each virgin reloading stress point.

Figures 3a and b show typical time histories of σ_a, ε_a and ε_r obtained, respectively, from a creep test and a delayed rebound test performed on HOS12. In Fig. 3a, the alphabet 'C' of C2 stands for creep test and the numeral *2* corresponds to the state represented by the encircled *2* shown in Fig. 2a, representing the stress state at which the creep test C2 was performed.

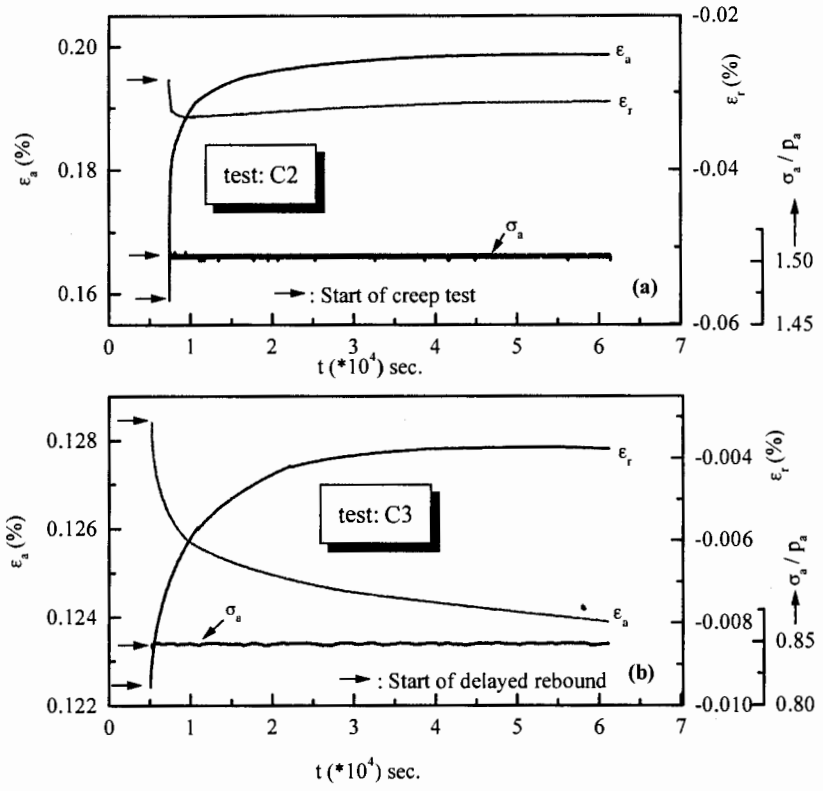

Fig. 3. Time histories of σ_a, ε_a, and ε_r during (a) creep, and (b) delayed rebound

Similarly, test C3 of Fig. 3b is representing a delayed rebound test performed at stress-state *3* in Fig. 2a after unloading along 2-3 stress-segment. The instant when the respective constant σ_a stage of creep test started is indicated by a horizontal arrow. Data for other similar creep / delayed rebound tests are available in Hoque (1996). In all the figures, the quantities— elapsed time, σ_a, etc.— were initialized at the beginning of shearing at point '0'. In the figures associated with small strain changes such as Fig. 3b, time histories of ε_a and ε_r were replaced by average smooth curves. This is because, the time histories were perturbed by the bit precision of the analogue-to-digital card and the resolution of the transducers (i.e., LDTs). The asteric (*) symbols in stress segments 2-3, 5-6 and 8-9 show, approximately, the stress locations at which CYL was applied to measure the axial elastic Young's modulus E^e and the Poisson's ratio ν. In CYL tests, the single amplitude axial strain was kept within 0.002%.

It can be observed that creep rate was quite large at the beginning of each creep stage, gradually decreased with time, and finally more-or-less died out. The behaviour was similar in both major and minor principal strains. The direction of creep was always in the direction of the recent deformation. That is, when a creep test was followed by a segmental shear in TC, ε_a was compressive during creep as it was in TC, while similarly ε_r was dilative (Fig. 3a). Conversely, in a delayed rebound test after unloading, ε_a was dilative and ε_r was compressive (Fig. 3b). The rate of delayed rebound exhibited the similar behaviour as creep did: that is, the rate was initially large, gradually decreased with time, and finally it became a negligible value. However, even at the beginning, the rate of delayed rebound rate was very small compared to that of creep rate at the same stress level.

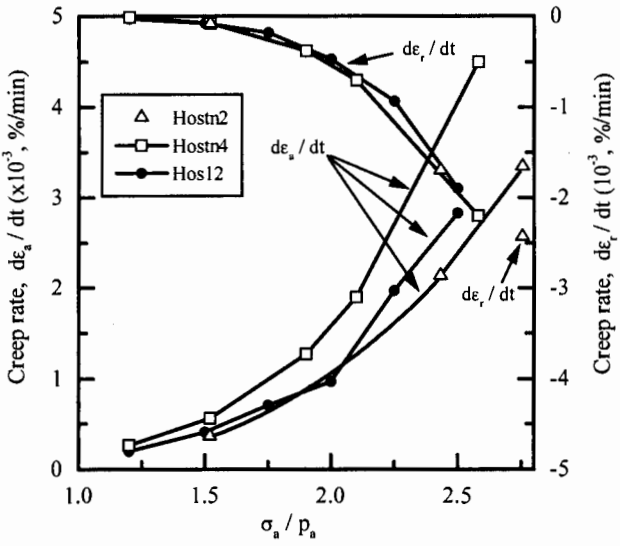

Fig. 4. Relationships between creep rates and σ_a

It is mentioned that the creep rate was not constant with time. However, for comparison, the average creep rate was estimated based on the total creep deformation that occurred during the first one hour. Figure 4 shows the relationships of creep rates in axial (i.e., $d\varepsilon_a/dt$) and radial (i.e., $d\varepsilon_r/dt$) directions with σ_a. The creep rate increased non-linearly with the increase in σ_a; the rate of increase augmented with the increase in the axial stress level. At a given stress state, the looser the specimen the larger was the creep rate in the direction of ε_a. The creep rate in the direction of ε_r (i.e., $d\varepsilon_r/dt$) was insensitive to the void ratio of specimen.

Figures 5a, b and c show the stress-dilatancy relationships of HOS12, HOSTN4, and HOSTN2 specimens, respectively. In these figures, the stress ratio R ($=\sigma_a/\sigma_r$) is plotted against the dilatancy rate D, where D is defined as the ratio of minor-to-major principal plastic strain increments. That is, for loading (σ_a increasing at constant σ_r), $D= -2d\varepsilon_r^p / d\varepsilon_a^p$ and for unloading (i.e., σ_a decreasing at constant σ_r) $D= -d\varepsilon_a^p / (2d\varepsilon_r^p)$, where $d\varepsilon_a^p$ and $d\varepsilon_r^p$ are the plastic strain increments in axial and radial directions, respectively. The elastic strain increments ($d\varepsilon_a^e$, $d\varepsilon_r^e$) are subtracted from the total strain increments (i.e., $d\varepsilon_a$, $d\varepsilon_r$ in Figs. 2a and b) to obtain the plastic strain increments (i.e., $d\varepsilon_a^p$, $d\varepsilon_r^p$). For that purpose, $d\varepsilon_a^e$ and $d\varepsilon_r^e$ were evaluated as $d\varepsilon_a^e= d\varepsilon_a/E^e$ and $d\varepsilon_r^e= -\nu x\, d\varepsilon_a^e= -\nu x\, d\varepsilon_a/E^e$, respectively. In so doing, the stress level-dependency of elastic Young's modulus E^e [i.e., $E^e= E_1 \times f(e) \times \sigma_a^m$] and Poisson's ratio ν [i.e., $\nu = \nu_0 \times (\sigma_a/\sigma_r)^{m/2}$] described in Hoque and Tatsuoka (1998) was used. In the above equations, various entities used are: a void ratio function $f(e)= (2.17 - e)^2 / (1+e)$ to account for the change in void ratio in course of testing in complicated stress paths; $E_1= E^e$ measured at $\sigma_a= 98$ kPa when $f(e)= 1$ (i.e., for $e= 0.82$); $\nu_0=$ average ν measured at isotropic stress-state and $m < 1.0$, a nonlinear exponent relating σ_a with E^e (Hoque and Tatsuoka, 1998). The elastic parameters E_1, ν_0, and m for the respective specimens were listed in Table 1. Note that the elastic parameters were evaluated by applying very small amplitude cyclic loads at various stress states during performing the complicated stress path tests described above.

In the figures, for each specimen, the stress-dilatancy relationships are plotted for deformations during: i) virgin (primary) loading from the initial stress point 0 to the maximum σ_a; ii) unloading along a typical stress segment (e.g., segment 8-9 of Fig. 2a); iii) creep tests using loading criteria of D (i.e., $D= -2d\varepsilon_r^p / d\varepsilon_a^p$); and iv) delayed rebound tests using the unloading criteria of D [i.e., $D= -d\varepsilon_a^p / (2d\varepsilon_r^p)$]. During a creep test and a delayed rebound test, it was reasonably assumed that the deformations were fully plastic (i.e., no elastic strain components). A few deviating data points, which are perhaps owing to lack of reliability, at the start of loading and/or at the start of unloading were discarded; particularly at the start of unloading, the deformation was nearly elastic for relatively a large stress increment, and therefore, the dilatancy data at that stress range was totally unreliable because of the very small values of plastic strain components.

Thus, for the primary loading, the stress-dilatancy relationship (i.e., R~D) was more-or-less linear for the investigated stress range. That is, Rowe's (1962) stress-dilatancy relation, $R= K.D$, is valid for Hostun sand specimens with $K= 2.60$, 2.68 and 3.20 for HOS12, HOSTN2 and HOSTN4, respectively. This indicates that the looser the specimen, the higher was the value of K. For a given R, the loose

specimen was more contractant (i.e., small D) than the denser one. The value of K depends on the kinematics of particle movement as the soil deforms. $K = W_i / W_o$, where W_i is the input plastic work done by the major principal stress ($=\sigma_a . d\varepsilon_a^p$ for loading in triaxial test) and W_o is the output plastic work against minor and intermediate principal stresses ($=-2\sigma_r . d\sigma_r^p$ for loading in triaxial test).

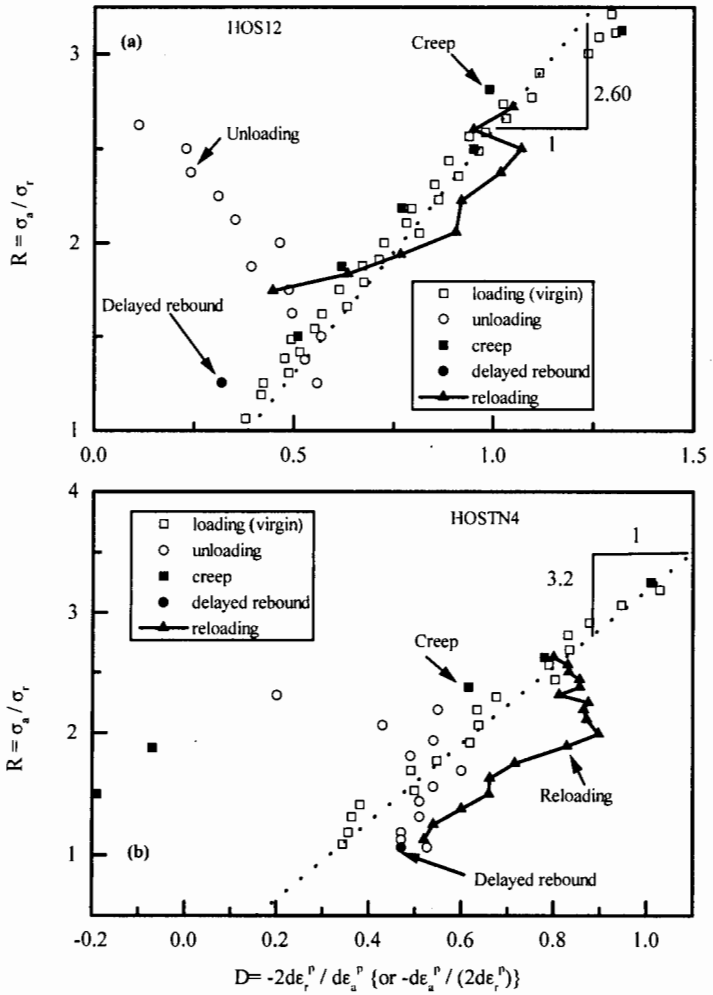

Fig. 5. Stress- dilatancy relationships for (a) HOS12 and (b) HOSTN4

Therefore, the value of energy ratio, K, depends on the percentage of W_i that is dissipated. For energy dissipated by sliding at particle

contacts, the value of K depends on the average orientation of sliding contacts, with respect to the principal stress directions, and on the mineral friction angle. When deformation takes place in the way that dissipates the smallest percentage of W_i, the stress-dilatancy coefficient K has its minimum value. The value of K is larger when the shear deformation becomes large, and is the maximum when the material ceases to change volume as it deforms, which is called the critical state. This discussion infers that the value of K is likely to be larger for a looser specimen.

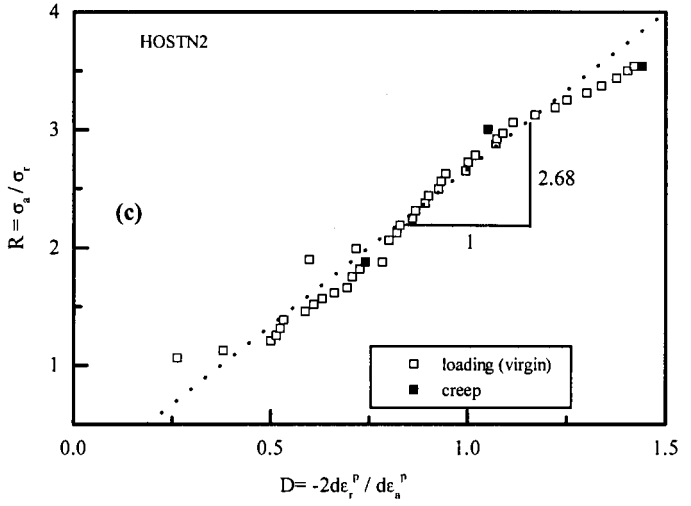

Fig. 5. Stress- dilatancy relationships for HOSTN2

The stress-dilatancy relationship during creep was nearly the same as that for virgin loading. However, some exception can be observed at low stress level, especially in the case of HOSTN4 specimen, in which the material exhibited relatively larger contractancy (i.e., small D). During reloading, the deformation at a given R became more dilatant (i.e., larger D) than that for virgin loading, while the slope K remained more-or-less similar to that for virgin loading (except the initial points in Fig. 2a). However, as R approached the previous maximum value after which the stress state was virgin, the value of D decreased, and eventually meet the value for virgin loading.

It should be mentioned that the stress-dilatancy relationships for unloading (and also for deformations during delayed rebound) are not plotted directly in a comparable form to that of loading (note that the creep deformation was also categorised as loading). That is, for unloading, the stress-ratio should be plotted in the inverse way (i..e., $1/R$~D). However, it can be easily seen that in such a case all the data points for unloading would fall well below and right to the extended

dotted line (up to R=0.4) that assume the R~D relationship of virgin loading linearly. This indicates that during unloading the deformation was more dilative (i.e., the larger D) than that would occur at a given R during loading.

CONCLUSIONS

For sand, deformation for a given span of time at a constant stress state after loading in triaxial compression, known as creep, was observed to increase with the increase in the shear stress level during monotonic loading. Direction of creep was always in the direction of the principal strains that occurred during the recently experienced loading. Rate of creep in the major principal strain was larger than that in the minor principal strain direction irrespective of void ratio. Deformation at a constant stress state after unloading, known as delayed rebound, also behaved in the similar way, but the magnitude of delayed rebound was, however, much smaller than that of creep at the same stress state.

Creep deformation followed Rowe's stress-dilatancy relationship (i.e., R= $K.D$) during virgin (primary) loading. However, the sand became more dilative (i.e., large D) at a given R during unloading (i.e., σ_a decreasing at constant σ_r). Therefore, the stress-dilatancy relationships during loading and unloading were not identical. Dilatancy rate during delayed rebound was more-or-less similar to that occurred during unloading at the same stress state.

REFERENCES

Hoque, E. (1996). "Elastic deformation of sands in triaxial sands," Ph.D. thesis, Tokyo Univ., 334p.

Hoque, E. and Tatsuoka, F. (1998). "Anisotropy in elastic deformation of granular materials," Soils and Foundations, Tokyo, Vol. 38, No. 1, pp. 163-179.

Hoque, E. and Tatsuoka, F. (2004). "Triaxial testing system for measuring loading-rate effects during cyclic tests of sand," Geotechnical Testing Journal, ASTM, to appear.

Goto, S., Tatsuoka, F., Shibuya, S., Kim, Y-S., and Sato, Y. (1991). "A Simple Gauge for Local Small Strain Measurements in the Laboratory," Soils and Foundations, Vol. 31, No. 1, pp. 169-180.

Mitchell, J.K. (1964). "Shearing resistance of soils as a rate process," J. Soil Mech. Fdn Engng Div., ASCE, 90-1, 29-61.

Olszak, W. and Perzyna, P. (1966). "On elasto / visco-plastic soils," Proc. IUTAM Symp. on Rheology and Soil Mechanics, Grenoble (Berlin: Springer-Verlag), pp. 47-57.

Perzyna, P. (1963). "The constitutive equations for rate sensitive plastic materials," Quarterly of Applied Maths, 20-4, 321-332.

Richardson, A.M. and Whitman, R.V. (1963). "Effect of strain rate upon drained shear resistance of a saturated remoulded fat clay," Geotechnique,, 13-4, 310-324.

Rowe, P.W. (1962). "Stress-dilatancy relation for state equilibrium of an assembly of particles in contact," Proceedings Royal Society, 269A, pp. 500-527.

Tatsuoka, F., Jardine R.J., Lo Presti, D., Di Benedetto, H. and Kodaka, T. (1997). "Characterizing the pre-failure deformation properties of geomaterials," Theme Lecture for the Plenary Session No. 1, 14th Int. Conf. On SMFE, Hamburg, Vol. 2.

Wood, D.M. (1990). "Soil behaviour and critical state soil mechanics," Cambridge University Press, London.